processes

MDPI

Article

TRIZ-Assisted Structural Design of a Polishing Machine for Aluminum Strip Straightening Rolls

Yanjuan Wang [1], Xiaoqing Hu [1], Junye Li [2], Zhiyuan Xu [3] and Leijie Fu [4,*]

[1] School of Intelligent Science and Engineering, Yantai Nanshan University, Longkou 265700, China
[2] College of Mechanical and Electrical Engineering, Xinjiang Agricultural University, Urumqi 830052, China
[3] Shandong Nanshan Aluminium Co., Ltd., Longkou 265700, China
[4] School of Mechatronic Engineering, Xi'an Technological University, Xi'an 710021, China
* Correspondence: fuleijie@vip.163.com

Abstract

Straightening rolls used in aluminum strip production are progressively contaminated by metal particles and fine debris that adhere to their surfaces. Periodic polishing is therefore required to restore the surface condition of the rolls while avoiding excessive material removal or surface damage. This study developed an automated polishing machine for aluminum strip straightening rolls using the Theory of Inventive Problem Solving (TRIZ) as a systematic engineering-design framework. Two engineering problems were considered: achieving effective contaminant removal without degrading the roll surface and improving loading and unloading productivity without introducing excessive device complexity. The problems were formalized using TRIZ engineering parameters and a contradiction matrix, after which candidate inventive principles were screened according to the physical requirements of the polishing process. The contradiction matrix was therefore used as a candidate-generation tool and engineering screening as the selection criterion. Based on the resulting design requirements, the machine was configured with an abrasive-belt feed mechanism, a lifting mechanism, and an automated loading and unloading mechanism. A programmable logic controller, servo and stepper drives, and an abrasive-belt system were integrated to coordinate workpiece positioning and polishing. A physical prototype was fabricated and evaluated using a two-group comparative test against manual polishing. Surface roughness was measured at three axial positions using a Surftest SJ-210 portable surface roughness tester. In this workshop-scale comparison of three rolls per method, machine-polished rolls exhibited lower mean Ra values and markedly smaller scatter than manually polished rolls, with 0.075 ± 0.004 μm compared with 0.951 ± 0.179 μm. Workshop records indicate an increase in polishing throughput from approximately 55 to 165 rolls/month. All nine machine-polished measurements satisfied the workshop acceptance criterion of Ra ≤ 0.6 μm, whereas all nine manually polished measurements exceeded it. These observations support the engineering feasibility of the proposed machine architecture under the investigated conditions.

Keywords: TRIZ; contradiction matrix; abrasive-belt polishing; straightening roll; polishing machine

Check for updates

Academic Editor: Jose Carlos Pinto

Received: 11 September 2026
Revised: 10 October 2026
Accepted: 12 October 2026
Published: 14 October 2026

Copyright: © 2026 by the authors. Licensee MDPI, Basel, Switzerland. This article is an open access article distributed under the terms and conditions of the Creative Commons Attribution (CC BY) license.

1. Introduction

The surface condition of working rolls is an important factor in strip-processing quality because roll topography and surface degradation can be transferred to, or otherwise affect, the processed material. Recent rolling studies have demonstrated that changes in work-roll

surface topography can alter the surface characteristics and mechanical response of thin metallic strips, while industrial straightening rolls are also subject to progressive wear under repeated rolling and sliding contact [1,2]. These observations indicate that the condition of a straightening-roll surface should be treated as a functional manufacturing variable rather than merely as a maintenance issue. For straightening rolls used in aluminum strip production, adhered metal particles, fine debris, and progressive surface deterioration therefore require periodic surface treatment to maintain an appropriate working surface.

Grinding and polishing of large metallic components are still frequently performed manually because manual tools are inexpensive and adaptable to different workpieces. However, manual polishing is inherently dependent on operator experience, posture, applied force, and local judgment, which makes it difficult to maintain consistent material removal over a long surface. Recent reviews of robot-assisted polishing and robotic abrasive-belt grinding show that the research focus has consequently shifted toward automated systems that combine controlled tool motion, force regulation, process sensing, and surface-quality evaluation [3,4]. These developments demonstrate the feasibility of replacing strongly operator-dependent finishing operations with controlled mechanical processes, but they also show that polishing quality remains sensitive to the interaction among machine stiffness, contact mechanics, tool trajectory, abrasive condition, and process parameters.

Among available finishing technologies, abrasive-belt grinding is particularly attractive for surface finishing because the compliant belt can accommodate local geometric deviations while maintaining a relatively large contact region. Nevertheless, belt compliance also makes material removal more difficult to predict than in rigid-tool machining. Recent studies have shown that surface formation and surface integrity depend on the dynamic interaction among abrasive grains, the compliant backing, the contact wheel, and the workpiece [5]. The relationship between normal force and actual removal depth is nonlinear because elastic deformation occurs within the grinding contact [6]. In addition, smooth trajectory generation and stable force regulation are required to avoid force overshoot and local surface deterioration [7]. Adaptive process optimization based on online surface information can further improve material-removal consistency [8], while precise contact-force control has been shown to improve both polishing stability and final surface roughness [9]. Investigations of variable-inclination belt grinding and grain-scale material-removal mechanisms have similarly demonstrated that force distribution, abrasive geometry, and local contact conditions are central to controlling surface integrity [10,11].

More recent work has increasingly integrated mechanical design with active compliance, sensing, and adaptive control. Li et al. developed a multi-tool robotic system combined with variable impedance control for grinding and polishing complex blade features [12]. Chen et al. introduced a two-degree-of-freedom active compliant end-effector to improve force-control accuracy during curved-surface grinding [13], while Li et al. examined compliant-tool optimization for complex surfaces under confined machining conditions [14]. Process stability is also affected by the abrasive tool itself. Image-based monitoring has been used to identify abrasive-belt wear states during grinding [15], and wear-evolution models have demonstrated that changes in structured abrasive belts directly modify material-removal behavior and surface roughness [16]. More recently, integrated robotic polishing platforms have combined machine vision, constant-force control, process planning, and multivariable roughness prediction within a single machining system [17]. Collectively, these studies show that high-quality automated finishing depends not on a single component or control parameter, but on coordinated control of contact force, relative motion, abrasive condition, workpiece positioning, and process sequencing.

However, the most recent literature has concentrated on robotic finishing of geometrically complex and high-value components such as aero-engine blades, blisks, weld seams,

and large free-form surfaces. The engineering requirements for straightening-roll polishing are different. The workpiece geometry is comparatively simple, but the rolls are long and relatively heavy, and an industrial machine must integrate loading, lifting, centering, rotation, abrasive-belt feeding, axial traversal, and unloading while maintaining consistent contact conditions along the working surface. Introducing additional automation can increase productivity, but it also increases the number of actuators, transmission elements, and control functions. Likewise, increasing abrasive action can improve contaminant removal but may increase unnecessary material removal or surface damage. The design problem is therefore characterized by competing engineering requirements rather than by polishing-process optimization alone.

The Theory of Inventive Problem Solving (TRIZ) provides a structured means of formulating such competing requirements as engineering contradictions and generating candidate solution principles. Recent reviews show that TRIZ continues to be used for engineering-system evolution, systematic innovation, and computer-aided design support, while also identifying the need to link generic inventive principles more explicitly to engineering implementation [18]. Computational design studies have shown that TRIZ can support problem structuring and design exploration when conflicting objectives must be considered simultaneously [19]. TRIZ-based contradiction analysis has also been incorporated into recent product-design methodologies to translate competing functional requirements into alternative design concepts [20]. These studies support the use of TRIZ as a problem-formulation and concept-generation framework rather than as a substitute for detailed mechanical design or experimental validation.

Accordingly, this study applies TRIZ-assisted engineering design to develop an automated polishing machine for aluminum strip straightening rolls. Two design problems are considered: maintaining effective surface polishing while limiting undesirable surface deterioration, and improving loading and unloading productivity without introducing unnecessary device complexity. The resulting concepts are implemented through an abrasive-belt feed mechanism, a lifting mechanism, an automated loading and unloading mechanism, and coordinated workpiece positioning and motion control. A physical prototype is subsequently fabricated and evaluated under workshop conditions by comparing the surface roughness of machine-polished and manually polished straightening rolls. The objective is not to propose a new TRIZ theory or a general robotic-polishing algorithm, but to examine whether a contradiction-driven design process can be translated into a workable industrial machine architecture for straightening-roll polishing.

2. System Description

The proposed straightening-roll polishing machine consists of three principal subsystems: an abrasive-belt feed mechanism, a lifting mechanism, and a loading and unloading mechanism.

The abrasive-belt feed mechanism provides the polishing action and the controlled radial and axial motions required to cover the roll surface. An abrasive-belt drive motor generates the belt motion, while the feed drive positions the abrasive-belt assembly relative to the workpiece. A tensioning structure maintains the required belt tension and contact condition.

The lifting mechanism raises the straightening roll from the loading position to the spindle axis. It provides vertical positioning before the roll is positioned between the spindle center and the tailstock center.

The loading and unloading mechanism transfers straightening rolls among the storage, machining, and completed-workpiece areas. A motor-driven chain-and-sprocket system

transports each roll toward the machining station. Guide elements position the roll for lifting. After polishing, the roll is lowered and transferred to the unloading area.

During operation, a straightening roll is first transported to the machining station by the loading mechanism. The lifting mechanism then raises the roll until its axis is aligned with the spindle axis. The tailstock advances, and the roll is positioned between the spindle center and the tailstock center. A hollow three-jaw chuck subsequently transmits spindle rotation to the workpiece while maintaining the required alignment.

After the workpiece has been positioned, the abrasive-belt feed mechanism moves toward the roll until the required contact condition is established. The spindle rotates the roll, the abrasive belt provides the polishing motion, and the feed mechanism traverses along the workpiece to cover the required axial region.

After polishing, the abrasive-belt mechanism retracts, the chuck releases the workpiece, and the tailstock moves away. The lifting mechanism lowers the straightening roll onto the unloading guide structure, after which the roll is transferred to the completed-workpiece area.

3. TRIZ-Assisted Structural Design of the Polishing Machine

3.1. Problem Formulation

During aluminum strip straightening, direct contact occurs between the strip and the straightening rolls. Metal particles and fine debris can consequently adhere to the roll surfaces, reducing surface quality and potentially affecting the quality of the processed strip. A dedicated polishing machine is therefore required to remove these contaminants while maintaining the surface condition of the rolls.

Based on the machining requirements and operating conditions, two engineering problems were identified.

The first problem concerns surface treatment. The polishing system must provide sufficient abrasive action to remove adhered contaminants, while excessive contact force, material removal, or unstable motion may degrade the roll surface.

The second problem concerns material handling. Increasing loading and unloading productivity generally requires additional actuators, transmission elements, and control functions, which may increase device complexity.

The first problem was treated as the primary design problem because it directly determines whether the machine can satisfy the polishing requirement. The second problem was treated as a supporting automation problem. Both were analyzed using TRIZ contradiction analysis.

3.2. TRIZ Contradiction Analysis

In TRIZ, a technical contradiction describes a situation in which an improvement in one engineering characteristic causes a deterioration in another. The contradiction-analysis procedure used in this study consisted of three steps. First, each engineering problem was expressed in terms of an improving parameter and a worsening parameter. Second, the corresponding contradiction-matrix entry was queried to identify candidate inventive principles. Third, the candidate principles were screened according to the physical requirements and structural constraints of the polishing machine.

For the surface-treatment problem, the desired improvement was mapped to Manufacturing Precision (engineering parameter 29), whereas the undesirable consequence was mapped to Loss of Time (engineering parameter 25). This matrix cell yielded the candidate inventive principles 32, 26, 28, and 18.

Principle 32 (Color Change) and Principle 26 (Copying) were rejected because neither has a physical counterpart in abrasive removal or in the mechanical structure of the

machine. Principle 28 (Mechanics Substitution) was not applied to this problem because substituting mechanical action with electrical or control action does not by itself constrain material removal; it was retained for the material-handling contradiction instead. Principle 18 (Mechanical Vibration) was rejected because superimposed vibration increases abrasive action and therefore conflicts with the requirement of limiting unnecessary material removal and surface damage. Because the contradiction between improving parameter 29 and worsening parameter 25 is fundamentally a matter of the duration and repetition of the contact, Inventive Principle 19: Periodic Action was introduced during engineering screening as a supplementary principle and was adopted to organize the repeated coordination of abrasive-belt motion, feed motion, and roll rotation. The criterion for its adoption is the temporal structure of the polishing contact: the operation requires repeatable, time-controlled passes under predefined conditions.

For the material-handling problem, the improving parameter was defined as Productivity (engineering parameter 39), whereas the worsening parameter was defined as Device Complexity (engineering parameter 36). This matrix cell yielded the candidate inventive principles 6, 12, 10, 1, 28, 27, 17, and 31.

Among the candidate principles, Inventive Principle 17: Another Dimension provides a direct conceptual basis for the lifting mechanism because the straightening roll is transferred vertically from the loading level to the spindle axis. The overall automation concept also incorporates electrical and electronic control functions in place of some manually executed mechanical operations, which is consistent with the general direction of Inventive Principle 28: Mechanics Substitution. The remaining candidates 6, 12, 10, 1, 27, and 31 imply segmented, spherical, or pneumatic structures that would add mechanical complexity without improving the vertical transfer of the workpiece or reducing manual handling. The rationale for the principles adopted from this cell is given in Table 1.

Table 1. TRIZ contradiction analysis and mapping of the adopted principles to the structural design.

Engineering Problem	Contradiction Parameters (Improving/Worsening)	Candidate Principles from the Matrix	Screening Rationale	Adopted Principle(s)	Resulting Design Feature
Contaminant removal without degrading the roll surface	Manufacturing Precision (29)/Loss of Time (25)	32, 26, 28, 18	32 and 26 have no physical counterpart in abrasive removal; 28 does not constrain material removal; 18 conflicts with limiting surface damage. The contradiction concerns the duration and repetition of the contact.	19 (Periodic Action), introduced as a supplementary principle	Coordinated roll rotation, abrasive-belt motion and axial feed in repeated passes
Higher loading and unloading productivity without excessive device complexity	Productivity (39)/Device Complexity (36)	6, 12, 10, 1, 28, 27, 17, 31	17 matches the vertical transfer between the loading level and the spindle axis; 28 matches the replacement of manually executed operations by electrical and electronic control; the material-handling design is therefore based on principles 17 and 28.	17 (Another Dimension), 28 (Mechanics Substitution)	Lifting mechanism transferring the roll vertically to the spindle axis; automated loading and unloading with PLC-controlled actuation

Table 1 summarizes the contradiction parameters, the matrix-listed candidate principles, the screening rationale, and the resulting design features for both engineering problems.

3.3. Structural Design

The resulting machine architecture consists of the abrasive-belt feed mechanism, lifting mechanism, loading and unloading mechanism, spindle and tailstock positioning system, and associated control system.

3.3.1. System-Component and Functional Analysis

A system-component analysis was conducted to identify the principal functional elements of the polishing machine. The machine was decomposed into subsystem components associated with abrasive-belt feeding, lifting, and workpiece transfer.The main components of each subsystem are listed in Table 2.

Table 2. Main components of the polishing machine.

System	Subsystem	Main Components
Polishing machine	Abrasive-belt feed mechanism	Sanding Belt (SaB) Feed Base (FB) Feed Motor (FM) Sanding Belt Motor (SBM) Hydraulic Rod (HR) Sanding Belt Wheel (SBW)
	Lifting mechanism	Lifting Screw (LS) Support Bearing (SuB) Cradle
	Loading and unloading mechanism	Loading Chain (LC) Loading Motor (LM) Sprocket Cutting Seat (CS) Unloading Screws (US)

The pairwise component interactions are represented in the component interaction matrix shown in Table 3. A "+" indicates a direct functional or mechanical interaction between two components, whereas a "−" indicates that no direct interaction is considered in the present model. The diagonal entries are omitted because a component is not compared with itself.

Table 3 presents the direct interaction relationships among the main components of the polishing machine. The matrix served to trace the transmission of motion and force among the subsystems and to identify the component pairs that govern the structural load paths; these pairs are examined quantitatively in Section 3.4.

Based on the component analysis, a functional model of the polishing machine was established, as shown in Figure 1. Electrical energy supplied to the drive motors is converted into the rotational and translational motions required for abrasive-belt polishing and workpiece handling.

A programmable logic controller (PLC) coordinates the principal actuators. Limit switches are installed at critical travel boundaries as safety devices. Servo and stepper drives are used to control workpiece positioning and feed motion. The principal polishing parameters include belt linear speed, feed speed, roll rotational speed, and grinding force.

Table 3. Component interaction matrix.

Component	SaB	FB	FM	SBM	HR	SBW	LS	SuB	Cradle	LC	LM	Sprocket	CS	US
SaB	—	+	–	+	–	+	–	–	–	–	–	–	–	–
FB	+	—	+	+	+	+	–	–	–	–	–	–	–	–
FM	–	+	—	–	–	–	–	–	–	–	–	–	–	–
SBM	+	+	–	—	–	+	–	–	–	–	–	–	–	–
HR	–	+	–	–	—	–	–	–	–	–	–	–	–	–
SBW	+	+	–	+	–	—	–	–	–	–	–	–	–	–
LS	–	–	–	–	–	–	—	–	+	–	–	–	–	–
SuB	–	–	–	–	–	–	–	—	+	–	–	–	–	–
Cradle	–	–	–	–	–	–	+	+	—	–	–	–	–	–
LC	–	–	–	–	–	–	–	–	–	—	+	+	–	–
LM	–	–	–	–	–	–	–	–	–	+	—	+	–	–
Sprocket	–	–	–	–	–	–	–	–	–	+	+	—	–	–
CS	–	–	–	–	–	–	–	–	–	–	–	–	—	+
US	–	–	–	–	–	–	–	–	–	–	–	–	+	—

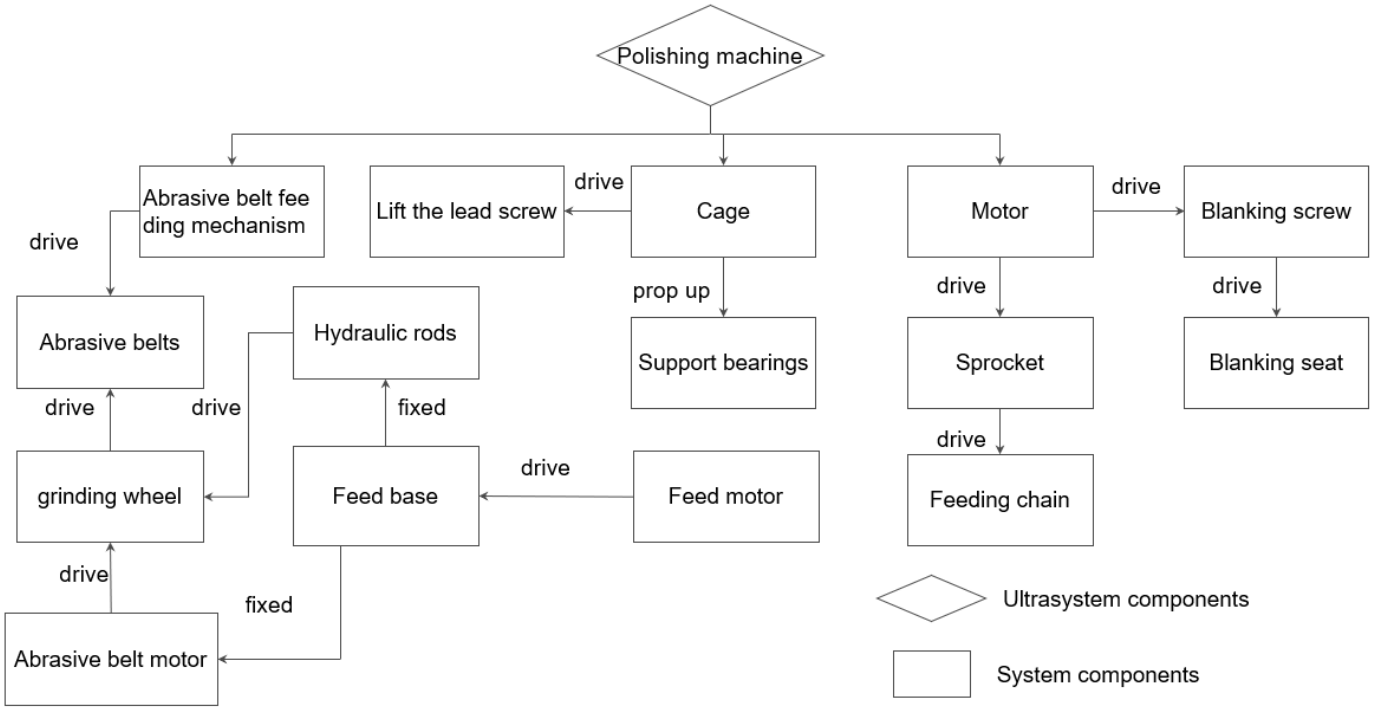


Figure 1. Functional model of the polishing machine.

3.3.2. Abrasive-Belt Feed Mechanism

The abrasive-belt feed mechanism was designed to provide repeatable polishing over the straightening-roll surface. The main structural frame is welded to provide sufficient structural rigidity.The structural configuration of the abrasive-belt feed mechanism is shown in Figure 2.

The abrasive-belt assembly is supported by cantilever structures arranged to provide access to the cylindrical workpiece. The belt path forms a V-shaped arrangement around the polishing region, increasing the available contact area while maintaining sufficient clearance for the roll.

An additional idler pulley is used for abrasive-belt tensioning. A hydraulic actuator provides the required tensioning or contact-support force. The complete abrasive-belt feed assembly is translated by a stepper-motor-driven screw mechanism so that the abrasive belt

can approach the roll, establish contact with its surface, traverse along the axial direction, and subsequently retract.

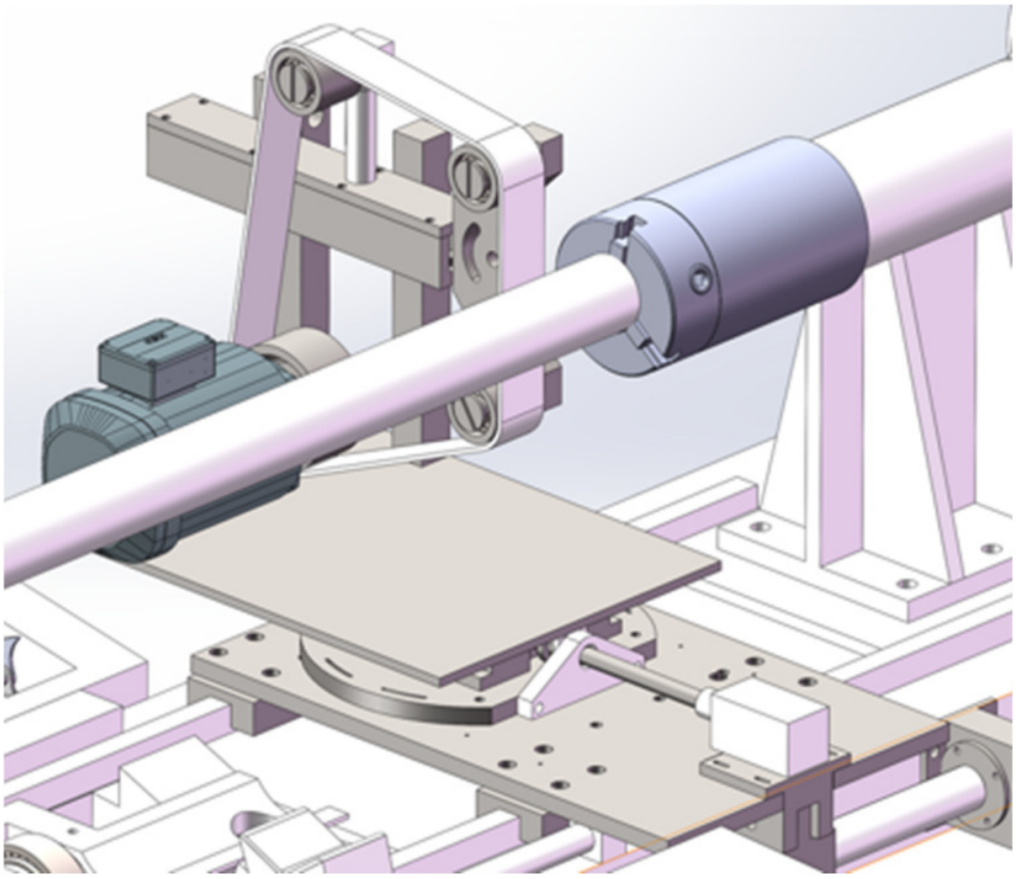


Figure 2. Structural configuration of the abrasive-belt feed mechanism.

The cyclic coordination of abrasive-belt motion, feed motion, and roll rotation provides repeated coverage of the target surface and reduces dependence on operator posture and manually applied force.

3.3.3. Lifting and Workpiece-Transfer Mechanisms

The lifting mechanism transfers the straightening roll vertically from the loading position to the spindle axis. A motor drives the lifting screw through the associated transmission structure. A roll support cradle mounted at the upper end of the lifting assembly supports the workpiece during vertical positioning.

Support bearings incorporated into the cradle reduce resistance during workpiece positioning and facilitate alignment with the spindle and tailstock centers. The overall structure of the lifting mechanism is shown in Figure 3.

The vertical transfer of the straightening roll provides the engineering implementation of Inventive Principle 17: Another Dimension. After the roll reaches the required height, it is positioned between the spindle center and the tailstock center before rotational motion is transmitted through the chuck.

The loading and unloading mechanism uses a chain-and-sprocket transmission and intermediate receiving structures to move the workpiece among the storage, machining, and completed-workpiece regions.

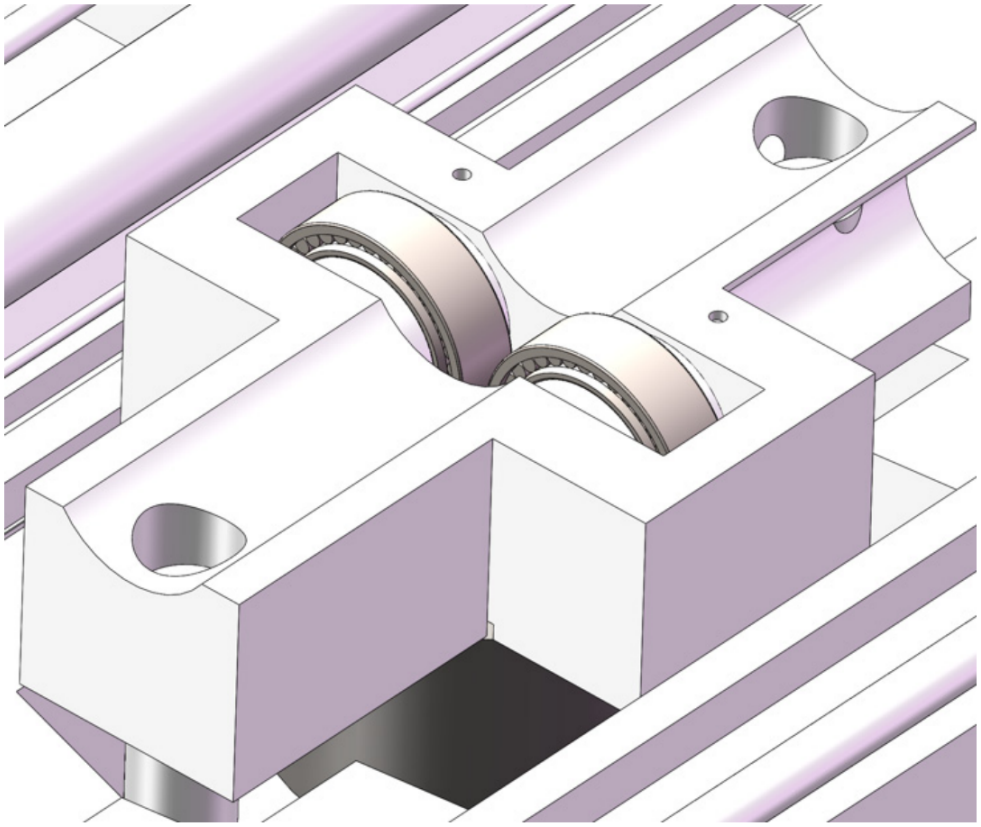


Figure 3. Lifting mechanism.

3.4. Analytical Design Checks of Principal Components

The principal mechanical and drive components were checked against the loads of the polishing operation; the values used are given in Table 4. Five load cases were considered. The abrasive-belt drive must generate the tangential force at the belt-roll contact within the rated torque and power of the drive motor. The belt-roll contact load, established by the abrasive-belt feed mechanism, is reacted by the spindle, the support bearings, and the frame, and is superimposed on the belt-tensioning force applied by the hydraulic cylinder through the tensioning pulley. The abrasive-belt feed screw carries the axial thrust, and the straightening roll and its cradle impose the vertical load that governs the lifting screw and the cradle support bearings. The unloading cantilever platform receives the polished roll after the polishing pass.

Table 4. Analytical design checks of the principal mechanical and drive components.

Component/Load Case	Governing Relation	Values Used
Abrasive-belt drive motor	$P = Ft \cdot vb$	A 2.2 kW induction motor
Abrasive-belt tensioning	$T \geq Ft$	Belt tension 60 N (Table 5); system rated pressure 5 MPa
Abrasive-belt feed screw	$F = \mu s \cdot m \cdot g$	T32 × 6 trapezoidal screw; feed thrust 153 N
Lifting screw	$\sigma = mg/A$	T30 × 6 trapezoidal screw; axial load 241 kg; σ = 5.7 MPa; f = 0.10, lead angle 4.1°, friction angle 5.9°
Spindle and cradle support bearings	C/P	6306 deep-groove ball bearings

Table 4. *Cont.*

Component/Load Case	Governing Relation	Values Used
Unloading cantilever platform	$\sigma = M/Wx$	Cast steel; 1300 N at a 400 mm overhang; 50 mm square section; safety factor 2 on the yield strength; σ = 25 MPa
Structural stiffness of the abrasive-belt feed frame	Static equilibrium of the feed assembly	The polishing assembly is carried on linear guideways; the frame reacts to the belt tensioning force and the contact force (Table 5)

Table 5. Polishing conditions, tool specifications and surface-roughness measurement protocol.

Parameter	Value
Prototype polishing	
Belt linear speed, vb (m/s)	15
Axial feed speed (mm/min)	100–200
Roll rotational speed (r/min)	60
Number of polishing passes per roll	1
Contact (normal) force between belt and roll, Fn (N)	30
Abrasive-belt tensioning	60 N, applied by a hydraulic tensioning cylinder; the hydraulic system is rated at a maximum pressure of 5 MPa
Nominal cycle time per roll	approximately 35 min
Abrasive belt	
Grit designation	1000 mesh
Abrasive grain material	Aluminum oxide (Al_2O_3)
Backing type	Cloth backing
Belt dimensions (width × length, mm)	60 × 1000
Manufacturer	3M Company, St. Paul, MN, USA
Manual polishing	
Procedure and tool	Handheld angle grinder with a 100-mesh wheel; endpoint determined by visual inspection
Operator experience	More than five years
Manual contact force	Controlled by the experience of the skilled operator
Working posture	The operator works in a sitting position and guides the angle grinder along the roll by hand
Nominal cycle time per roll	Approximately 120 min
Roughness measurement	
Instrument and method	Surftest SJ-210 portable surface roughness tester (Mitutoyo Corporation, Kawasaki, Japan), contact stylus method
Measurement positions	Three axial positions per roll, with at least three repeated measurements at each position
Surface acceptance criterion of the production workshop	$Ra \leq 0.6$ μm

The governing relations are as follows. The power at the belt drive is obtained from the tangential force at the polishing contact as P = Ft·vb. The belt tension must at least equal the tangential force transmitted at the contact, T ≥ Ft. The thrust needed to translate the belt assembly along its guideways is F = μs·m·g, where μs is the friction coefficient of the guideways and m is the sliding mass. The lifting screw is checked in compression by σ = mg/A, where A is the cross-sectional area of the screw, and the stress is compared with the allowable stress of the screw material. The cradle bearings are checked by the load ratio C/P, where C is the basic dynamic load rating, and P is the equivalent dynamic load. The unloading cantilever is checked in bending by σ = M/Wx, where M = F·l is the bending moment produced by the load F acting at the overhang l.

For the polishing pass reported here, the contact force is Fn = 30 N, the belt speed is vb = 15 m/s, and the belt tension is 60 N (Table 5).

4. Results and Discussion

4.1. Prototype Test Design

A physical prototype was fabricated to evaluate whether the proposed machine could polish straightening-roll surfaces under workshop conditions. Six straightening rolls were selected from the production workshop for the comparative test. The rolls had diameters of 40–80 mm and lengths of 2500–4000 mm and were made of 100Cr6 steel, giving an individual roll mass of approximately 25–157 kg. Three rolls were polished with the prototype machine and three manually, so that three rolls were assigned to each polishing method.

For the machine-polishing group, each roll was subjected to a single polishing pass with a 1000-mesh abrasive belt on the prototype machine; the principal parameters and the belt specification are given in Table 5. For the manual-polishing group, a handheld angle grinder with a 100-mesh wheel was used by an operator with more than five years of experience, following the existing workshop procedure and determining the endpoint by visual inspection; the tool, the working posture, and the cycle time are also summarized in Table 5.

Surface roughness was selected as the primary surface-quality metric and was measured by a qualified third-party testing organization with a Surftest SJ-210 portable surface roughness tester manufactured by Mitutoyo Measuring Instruments (Shanghai) Co., Ltd.(Shanghai, China), using the contact stylus method. The instrument has an X-axis measuring range of 16 mm and a detector range of −200 to +160 μm; the reported range/resolution combinations include 360 μm/0.02 μm and 100 μm/0.006 μm. Measurements were taken at three axial positions per roll, with at least three repeated measurements at each position. The rolls were polished in the condition in which they were received from the production line.

The surface contamination observed before polishing is shown in Figure 4.

4.2. Prototype Fabrication

The physical prototype was manufactured according to the structural design described above. The prototype integrates the abrasive-belt feed mechanism, the lifting mechanism, the spindle and tailstock positioning system, the loading and unloading mechanism, and the control system. The completed prototype is shown in Figure 5.



Figure 4. Surface contamination on a straightening roll before polishing. The red arrows indicate areas with visible surface discoloration and marks.



Figure 5. Physical prototype.

https://doi.org/10.3390/pr14203307

4.3. Prototype Test Results

The measured surface-roughness parameter Ra for the machine-polished and manually polished straightening rolls is reported in Tables 6 and 7.

Table 6. Surface roughness Ra of the machine-polished straightening rolls.

Workpiece	Front Section, Ra (μm)	Middle Section, Ra (μm)	Rear Section, Ra (μm)
1	0.079	0.075	0.075
2	0.073	0.078	0.075
3	0.081	0.069	0.073
Mean ± SD	0.078 ± 0.004	0.074 ± 0.005	0.074 ± 0.001

Table 7. Surface roughness Ra of the manually polished straightening rolls.

Workpiece	Front Section, Ra (μm)	Middle Section, Ra (μm)	Rear Section, Ra (μm)
4	0.81	0.92	0.73
5	1.15	0.82	0.90
6	0.85	1.23	1.15
Mean ± SD	0.937 ± 0.186	0.990 ± 0.214	0.927 ± 0.211

The tabulated measurements show a clear descriptive difference between the two polishing methods. For the machine-polishing group the mean Ra values were 0.078 ± 0.004, 0.074 ± 0.005 and 0.074 ± 0.001 μm at the front, middle and rear sections, respectively, with an overall mean of 0.075 ± 0.004 μm; for the manual-polishing group the corresponding values were 0.937 ± 0.186, 0.990 ± 0.214 and 0.927 ± 0.211 μm, with an overall mean of 0.951 ± 0.179 μm (Tables 6 and 7). The standard deviation across the three rolls at each axial position was smaller for machine polishing (≤0.005 μm) than for manual polishing (0.186–0.214 μm), which indicates better roll-to-roll repeatability. The spread of the mean values across the three axial positions was 0.0037 μm for machine polishing and 0.0633 μm for manual polishing, which indicates a more uniform surface finish along the roll.

During manual polishing, operators tend to concentrate on visibly contaminated regions. Because contaminant distribution is spatially nonuniform, local polishing time and applied force may vary substantially along the roll. Excessive local grinding may result in unnecessary material removal or local depressions, whereas insufficient treatment may leave portions of the surface inadequately processed.

In contrast, the prototype provides programmed workpiece rotation and abrasive-belt feed over the required axial range. The resulting motion reduces dependence on operator posture and manually applied force and provides more consistent coverage of the roll surface.

According to the production records of the workshop, polishing throughput increased from approximately 55 rolls/month with the previous manual procedure to approximately 165 rolls/month with the prototype machine, an approximately threefold improvement. The workshop operates three 8 h shifts per day, and the nominal cycle time per roll is approximately 120 min for the manual procedure and approximately 35 min for the prototype (Table 5). The records analyzed here cover April 2026.

Figure 6 further compares the surface-roughness measurements obtained for the machine-polished and manually polished workpieces.

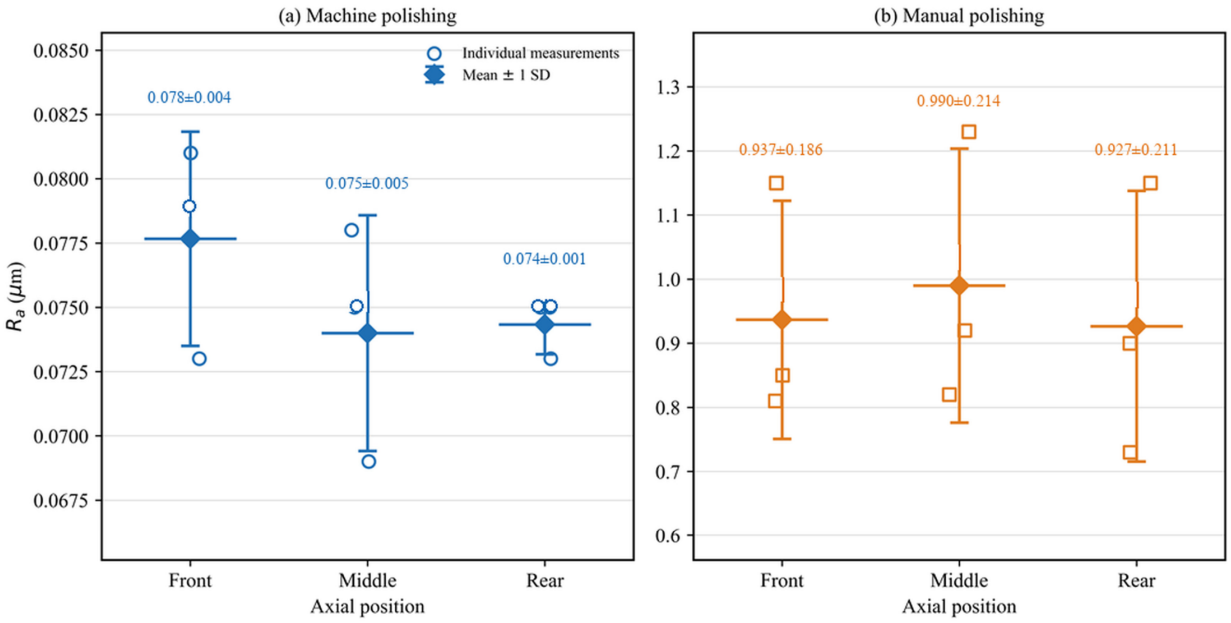


Figure 6. Surface roughness Ra of the machine-polished and manually polished straightening rolls at the front, middle, and rear axial sections. (**a**) Machine-polishing group, plotted on an expanded ordinate; (**b**) manual-polishing group. Symbols denote individual measurements, horizontal bars denote group means, and error bars denote ±1 standard deviation for the three measurements at each position.

Figure 6 compares the Ra values measured at the front, middle, and rear axial positions for the machine-polishing and manual-polishing groups. The two methods are plotted on separate ordinate scales so that the individual measurements, group means, and ±1 standard deviation error bars of both groups remain legible. At all three positions, the machine-polished straightening rolls exhibited substantially lower Ra values than the manually polished rolls. The per-position mean values are given in Tables 6 and 7.

The production workshop accepts straightening-roll surfaces against a surface-roughness limit of Ra $\leq$ 0.6 μm (Table 5), which is used as the primary surface-quality metric. Against this limit, all nine measurements of the machine-polished rolls, which ranged from 0.069 to 0.081 μm, meet the requirement, whereas all nine measurements of the manually polished rolls, which ranged from 0.73 to 1.23 μm, exceed the 0.6 μm limit.

Recent automated polishing systems achieve force-controlled and sensor-guided finishing of free-form components through robotic manipulation combined with adaptive path planning and material-removal modeling [3,4,12–17]. The present machine reduces the problem to the axisymmetric geometry of a cylindrical roll on a stiff two-axis platform, so that the conditions in Table 5 are held constant along the polished length. Measurements indicate that the machine reduces the scatter of Ra and increases production efficiency; a further reduction in manual effort and in the associated labor cost is anticipated.

5. Conclusions

This study developed an automated polishing machine for aluminum strip straightening rolls using a TRIZ-assisted engineering design approach. The design problem was divided into two primary tasks: controlled surface polishing and automated workpiece handling. TRIZ contradiction analysis was used to identify candidate inventive principles, and the resulting principles were incorporated into the structural design of the abrasive-belt feed mechanism, lifting mechanism, loading and unloading mechanism, spindle and tailstock positioning system, and programmable control system.

A physical prototype was fabricated and evaluated under workshop conditions. In this workshop-scale test, the machine-polished straightening rolls exhibited lower and more spatially uniform Ra values than the manually polished rolls. According to Tables 6 and 7, the standard deviation at each axial position was no more than 0.005 μm for the machine-polished rolls, whereas it was 0.186–0.214 μm for the manually polished rolls. Workshop records also indicated an increase in polishing throughput from approximately 55 to 165 rolls/month, and all nine machine-polished measurements satisfy the workshop acceptance criterion of Ra $\leq$ 0.6 μm. These observations establish the engineering feasibility of the proposed polishing machine for this application under the investigated operating conditions.

The validation reported here covers three rolls per polishing method and three axial positions per roll. The evaluation was performed on the production line, where the two groups differ by a factor of at least nine at every axial position; the reported values apply to the tested rolls and to the workshop conditions under which they were polished. A larger number of rolls and a controlled pre-polishing baseline, together with contaminant-removal effectiveness, dimensional change, roundness, cylindricity, processing time, and long-term repeatability, are the subjects of the follow-up validation.

Author Contributions: Y.W.: conceptualization, methodology, formal analysis, investigation, data curation, writing—original draft preparation, visualization, and project administration; X.H.: validation, investigation, data curation, and visualization; J.L.: methodology, formal analysis, and writing—review and editing; Z.X.: validation, investigation, and resources; L.F.: conceptualization, supervision, project administration, writing—review and editing, and funding acquisition. All authors have read and agreed to the published version of the manuscript.

Funding: This research was funded by the Nanshan Holdings Research Project, "Optimization Design of an Aluminum-Melt Dross-Skimming Robot Workstation" (Project No. 2025-6-1); the Nanshan Holdings Research Project, "Design and Fabrication of Wear- and Corrosion-Resistant Coatings for Key Equipment Used in Aluminum Alloy Casting" (Project No. 2026-6-4); and the Nanshan Holdings Research Project, "Optimization Design of an Aluminum Strip Straightening Roll Polishing Machine" (Project No. 2023-5-2).

Data Availability Statement: The data supporting the findings of this study are included within the article. The polishing parameters, surface-roughness measurements, and throughput records reported here are released by the industrial partner for publication in this article; the underlying production records are the property of the industrial partner. Certain production-related data are not publicly available because they contain information associated with the industrial production process.

Conflicts of Interest: Author Zhiyuan Xu was employed by the company Shandong Nanshan Aluminum Co., Ltd. He acted as the company-side responsible person for the industrial application and testing of the machine described in this study. The remaining authors declare that the research was conducted in the absence of any commercial or financial relationships that could be construed as a potential conflict of interest. The authors declare that this study received funding from Nanshan Holdings. The funder had the following involvement with the study: the provision of the industrial trial site and access to the production line, the supply of the straightening rolls used in the trial, and access to the workshop production records.

References

1. Zhang, Z.; Zhang, H.; Liu, X.; Wang, T.; Huang, Q.; Liao, X. Effect of roll surface topography on microstructure and mechanical properties of 304 stainless steel ultra-thin strip. *J. Manuf. Process.* **2023**, *108*, 764–778. [CrossRef]
2. Domitner, J.; Schneeberger, P.; Silvayeh, Z.; Schnideritsch, H.; Engel, J.K.; Schider, S.; Klarner, J. Experimental quantification of the wear performance of rolls used in industrial rotary straightening of seamless steel tubes. *Wear* **2025**, *578–579*, 206148. [CrossRef]

3. Ke, X.; Yu, Y.; Li, K.; Wang, T.; Zhong, B.; Wang, Z.; Kong, L.; Guo, J.; Huang, L.; Idir, M.; et al. Review on robot-assisted polishing: Status and future trends. *Robot. Comput.-Integr. Manuf.* **2023**, *80*, 102482. [CrossRef]
4. Zhang, B.; Wu, S.; Wang, D.; Yang, S.; Jiang, F.; Li, C. A review of surface quality control technology for robotic abrasive belt grinding of aero-engine blades. *Measurement* **2023**, *220*, 113381. [CrossRef]
5. Li, S.; Xiao, G.; Chen, B.; Zhuo, X.; Xu, J.; Huang, Y. Surface formation modeling and surface integrity research of normal ultrasonic assisted flexible abrasive belt grinding. *J. Manuf. Process.* **2022**, *80*, 232–246. [CrossRef]
6. Song, K.; Xiao, G.; Chen, S.; Liu, X.; Huang, Y. A new force-depth model for robotic abrasive belt grinding and confirmation by grinding of the Inconel 718 alloy. *Robot. Comput.-Integr. Manuf.* **2023**, *80*, 102483. [CrossRef]
7. Min, K.; Ni, F.; Liu, H. Robotic abrasive belt grinding of complex curved blades based on a novel force control architecture integrating smooth trajectories. *J. Manuf. Process.* **2023**, *107*, 447–458. [CrossRef]
8. Ge, J.; Deng, Z.; Li, Z.; Liu, T.; Zhuo, R.; Chen, X. Adaptive parameter optimization approach for robotic grinding of weld seam based on laser vision sensor. *Robot. Comput.-Integr. Manuf.* **2023**, *82*, 102540. [CrossRef]
9. Xie, F.; Chong, Z.; Liu, X.-J.; Zhao, H.; Wang, J. Precise and smooth contact force control for a hybrid mobile robot used in polishing. *Robot. Comput.-Integr. Manuf.* **2023**, *83*, 102573. [CrossRef]
10. Xiao, G.; Liu, X.; Song, K.; Zhang, T.; Huang, Y. Research on robotic belt grinding method of blisk for obtaining high surface integrity features with variable inclination angle force control. *Robot. Comput.-Integr. Manuf.* **2024**, *86*, 102680. [CrossRef]
11. Chu, Y.; Yan, S.; Yang, Z.; Xu, X.; Wang, H.; Ding, H. Grain shape-protrusion-based modeling and analysis of material removal in robotic belt grinding. *J. Manuf. Process.* **2024**, *110*, 211–223. [CrossRef]
12. Li, X.; Zhao, H.; Zhou, H.; Cai, Y.; Yin, Y.; Ding, H. Robotic grinding and polishing of complex aeroengine blades based on new device design and variable impedance control. *Robot. Comput.-Integr. Manuf.* **2025**, *92*, 102875. [CrossRef]
13. Chen, H.; Yang, J.; Ding, H. Robotic grinding of curved parts with two degrees of freedom active compliant force-controlled end-effector using decoupling control algorithm. *Robot. Comput.-Integr. Manuf.* **2025**, *93*, 102935. [CrossRef]
14. Li, M.; Wang, W.; Zou, L.; Lv, C.; Zhang, J.; Huang, Y. Robotic grinding of complex surfaces with an internal structured compliant tool: Multi-performance optimization in confined spaces. *Robot. Comput.-Integr. Manuf.* **2025**, *94*, 102974. [CrossRef]
15. Chen, B.; Chen, R.; Ding, Y.; Qi, J.; Wang, R. Image-based wear state evolution and in-process recognition method for abrasive belt grinding of GH4169. *J. Manuf. Process.* **2025**, *141*, 237–249. [CrossRef]
16. Liu, Y.; Wang, W.; Yan, S.; Wan, L.; Zou, L. Transformation of material removal behavior and its mechanism modeling with the wear evolution of pyramidal structured abrasive belts. *J. Manuf. Process.* **2025**, *137*, 125–134. [CrossRef]
17. Wu, D.; Li, H.; Wang, H.; To, S. Robotic abrasive cloth flap wheel polishing system and multivariate parameter decision-making method for blade leading and trailing edges. *Robot. Comput.-Integr. Manuf.* **2026**, *97*, 103075. [CrossRef]
18. Ghane, M.; Ang, M.C.; Cavallucci, D.; Abdul Kadir, R.; Ng, K.W.; Sorooshian, S. TRIZ trend of engineering system evolution: A review on applications, benefits, challenges and enhancement with computer-aided aspects. *Comput. Ind. Eng.* **2022**, *174*, 108833. [CrossRef]
19. Khodadadi, A.; von Buelow, P. Design exploration by using a genetic algorithm and the Theory of Inventive Problem Solving (TRIZ). *Autom. Constr.* **2022**, *141*, 104354. [CrossRef]
20. Rau, H.; Wu, J.-J.; Procopio, K.M. Exploring green product design through TRIZ methodology and the use of green features. *Comput. Ind. Eng.* **2023**, *180*, 109252. [CrossRef]

Disclaimer/Publisher's Note: The statements, opinions and data contained in all publications are solely those of the individual author(s) and contributor(s) and not of MDPI and/or the editor(s). MDPI and/or the editor(s) disclaim responsibility for any injury to people or property resulting from any ideas, methods, instructions or products referred to in the content.